

The effect of carrier gas humidity on the vaporization of laser-produced aerosols in inductively coupled plasmas

Cite this: DOI: 10.1039/c3ja50314c

Luca Flamigni,* Joachim Koch and Detlef Günther

In a recent study we reported on the discovery of an interrelationship between the kind of material sampled by laser ablation (LA) and the shape of OES profiles formed by atoms along the axis of an inductively coupled plasma (ICP), which is commonly used as an atomization and ionization source for mass spectrometry (MS). These results encouraged us to resume efforts on OES-based diagnostics to investigate vaporization-related elemental fractionation effects occurring during LA-ICP-MS and to conceive strategies for their suppression. Since the quantification capabilities and sensitivity of LA-ICP-MS tend to improve when water is simultaneously added to the carrier gas, we hypothesized that a matching of analyte/material-dependent points of vaporization in the ICP may be responsible for the increased accuracy that is often observed under such conditions. In this work, the impact of water admixture was investigated by side-on OES of an ICP using a Czerny–Turner monochromator operating in 2D imaging mode. Our data indicated a superposition of calcium- and sodium-specific OES axial profiles which were separated by several millimeters when no water was supplied, thus, supporting the hypothesis previously made. Furthermore, the utilization of a micro-droplet dispenser allowed to precisely adjust the amount of water entrained into the ICP and to specify the range of relative humidity required for matching the points of vaporization. Conditions specified this way were applied to quantitative LA-ICP-MS analyses of silicate glass and brass using matrix matched and non-matrix matched calibration, respectively, whereby the former resulted in significant improvements in the accuracy as well as lower detection limits with moderate increases of the oxide formation rate.

Received 25th September 2013

Accepted 11th November 2013

DOI: 10.1039/c3ja50314c

www.rsc.org/jaas

Introduction

When looking at the progress laser ablation inductively coupled plasma mass spectrometry (LA-ICP-MS) has undergone over the last decade it becomes obvious that most of the achievements made rely on instrument upgrades including both laser and ICP-MS equipment. In this conjunction, the utilization of laser systems providing femtosecond (fs) pulses or the design of high-throughput vacuum interfaces and mass/charge filters are only a few examples. By comparison, less efforts have been made to conceive quantification strategies that allow suppressing elemental fractionation and, therefore, to enhance the accuracy of analysis. As a matter of fact, analyses carried out by LA-ICP-MS are often subject to quantification errors due to the persistent lack of adequate reference materials requiring the utilization of non-matrix matched calibration standards.⁶ In order to improve the accuracy achievable under such conditions, in 2006, O'Connor *et al.*⁵ proposed the addition of water to the transport line of aerosols produced by nanosecond (ns)

LA; a concept which was recently adapted by Wälle *et al.*,⁷ who reported on LA-ICP-MS by non-matrix matched calibration applying fs laser pulses. To date, the improvement of accuracies found in ref. 5 and 7 remained an empirical finding although it was vaguely ascribed to a conditioning of the ICP properties, but no specific explanation about its real origin has yet been given.

The perfect set of preconditions for a material-independent and, thus, accurate analysis by LA-ICP-MS can be outlined as follows: first, aerosols produced by LA of both sample and standard are stoichiometric, *i.e.* match the composition of the bulk material, and are transported loss-free; this condition may be met even if losses occur but requires the over-all composition of aerosols reaching the ICP to remain unchanged. Second, all aerosol particles entering the ICP vaporize at the same axial position and instantaneously, so that out-of-axis diffusion and, thus, sampling efficiencies – defined as the relative fraction η of the vaporized material passing through the sampler cone – are identical. Note that η does not necessarily need to be the same for all analytes as long as there is no relative difference of η between each analyte carried by sample and standard aerosol. Last, if analyte-specific ion yields are material-independent too, and no significant fractionation during the mass/charge separation of ions happens downstream the vacuum interface due

Swiss Federal Institute of Technology, Laboratory of Inorganic Chemistry, Wolfgang-Pauli-Straße 10, CH-8093 Zürich, Switzerland. E-mail: flamigni@inorg.chem.ethz.ch

to, *e.g.*, space charge-induced ion repulsion, all preconditions for an accurate analysis by LA-ICP-MS are fulfilled. Of course, a realization of all these conditions at once would be desirable but variations have been reported in several papers dealing with the fundamental aspects of LA-ICP-MS or are obvious in daily routine whenever analyses fail. Nevertheless, efforts are being made to get closer to this ideal and to conceive strategies for the improvement of the accuracy of the analyses. In the scope of this work, the second item was addressed and, therefore, resumes recent activities on the investigation and understanding of vaporization-related fractionation effects as, for instance, tackled in ref. 1 and 8.

One straightforward way of monitoring changes of ICP properties upon the addition of water is 2D optical emission spectrometry (OES) using interference filters offering the advantages of ease-of-use and high light throughput, *i.e.* sensitivity. In a recent study,¹ we installed such a system allowing us to investigate material-dependent vaporization processes of laser-produced aerosols entrained into ICP sources. A disadvantage of using standard interference filters is their broad bandwidth giving rise to spectral interferences and limiting the number of atomic lines accessible at a time. To overcome this limitation and to increase the spectral resolution, a Czerny–Turner monochromator was operated in 2D imaging mode by projecting a de-magnified image of the ICP onto the entrance slit and acquiring the spectrally decomposed image formed at the position of the exit slit through a re-magnifying objective, as described in ref. 9 and 10. With the help of this setup, the effect of water addition on the vaporization of laser-produced aerosols in the ICP was studied for sodium chloride and calcium chloride which served as examples of two fully oxidized metals with different boiling points. The results are presented for two water supply systems: a common nebulizer/spray chamber assembly and a micro-droplet dispenser^{11,12} whereby the latter gave a higher precision in the water supply and enabled us to reduce its amount significantly. Our data allowed determining the minimum amount of water required to match material-dependent axial positions of complete vaporization inside the ICP and, in addition, offered the feasibility of interpreting the observations made by O'Connor *et al.*⁵ and Wälle *et al.*⁷

In the course of our studies, the question arose whether the reduced amount of water would be sufficient to keep up the accuracy improvements found in ref. 4 and the increased sensitivity reported in ref. 5. Therefore, LA-ICP-MS analyses of brass and silicate glass were performed under low humidity conditions applying matrix matched and non-matrix matched calibration standards.

Experimental

2D OES imaging and LA-ICP-QMS

The imaging setup used is based on the studies by Olesik and Hieftje⁹ and Webb and Hieftje¹⁰ who proposed operating open-slit monochromators to obtain spectrally decomposed 2D images of emitting objects. In this study, the ICP of a commercial quadrupole (Q)MS instrument (ELAN 6000, Perkin

Elmer, Waltham, MA, USA) was de-magnified and projected onto the entrance port of a Czerny–Turner grating monochromator (Horiba Spex 1000, Kyoto, Japan) by means of an achromatic objective (Pentax, 100 mm, 1 : 2.8, Tokyo, Japan) which gave a spectral resolution of about 1.5 nm. To adapt to the aspect ratios of the ICP and the monochromator's entrance port, a periscope was positioned between the ICP and the monochromator which rendered an image rotation by 90°. The spectrally decomposed image formed at the plane of the monochromator exit port was then re-magnified by a macro zoom lens attached to either an ICCD camera (iStar DH734, Andor, Belfast, Northern Ireland) or a CCD camera (JAI M2, Stemmer Imaging GmbH, Puchheim, Bavaria, Germany) depending on the pixel resolution and exposure time needed. In order to keep the entire setup compact an object distance of about one meter was chosen resulting in a mismatch of imaging optics and monochromator numerical aperture and, thus, a decreased light throughput, though. However, the spectral bandwidth was narrowed by a factor of six to seven compared to that offered by standard interference filters, which enhanced the signal-to-background ratio and increased the image contrast at longer exposure times (>100 μ s). A precise alignment of the setup including grating and mirrors of the monochromator was facilitated by the radiation of a helium–neon laser and setting a corresponding wavelength of 632.8 nm. Prior to each measurement, the imaging system was first focused onto the RF coil of the ICP for size calibration of images

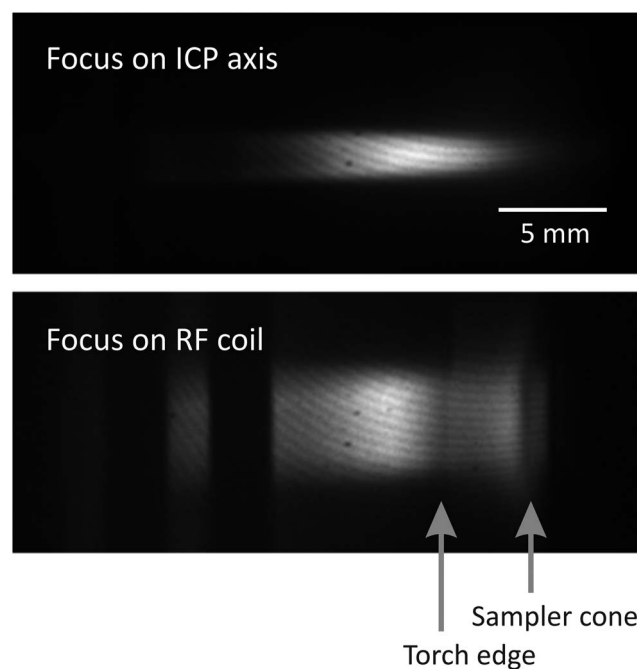


Fig. 1 Sodium atomic emission captured with the system focused onto the central channel of the plasma (top image) and onto the RF coil (bottom image). The bottom image was used for size calibration taking into account the width of the RF coil (3 mm), which is well visible on the left. On the bottom image, the edge of the quartz torch can be seen at about two third of the image from the left as well as the sampler cone at the end of the bright area.

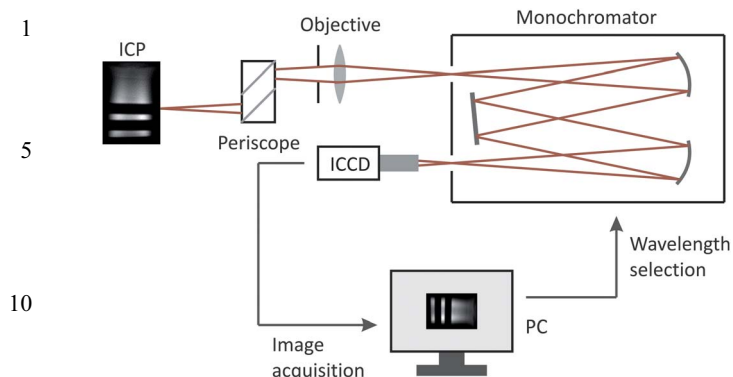


Fig. 2 Sketch of the monochromator-based 2D imaging setup used for OES mapping of an ICP.

acquired and then back onto the central channel of the ICP by moving the camera and objective with micrometer-precise translation stages. In Fig. 1, two pictures of the sodium atomic emission at 589 nm are shown, one with the system focused on the RF coil and the other one onto the central channel of the ICP.

The atomic emission of analytes was captured at 589 nm for sodium and 586 nm for calcium, whereas residual humidity was monitored using the hydrogen line at 656 nm. A sketch of the imaging setup is shown in Fig. 2. To study the influence of the humidity level on the achievable sensitivity, (Q)MS was performed with the same instrument. All system parameters including RF power, gas flow rates, and extraction lens voltage were kept constant at values of 1400 W, 0.8 L min⁻¹ argon plus 1.0 L min⁻¹ helium, and 7 V, respectively, to avoid any misinterpretation of data acquired. Note, that cooling and auxiliary gas flow rates for the Elan 6000 ICP-QMS instrument were preset by the manufacturer to values of 17 and 1.2 L min⁻¹. Aerosols were produced by LA using a pulsed nanosecond (ns) Nd:YAG laser system operating at a wavelength of 266 nm (LSX 500, Cetac Technologies, Omaha, NB, USA). Throughout OES measurements the LA protocol in terms of scan speed, laser repetition rate, spot size, and laser pulse energy determining

the amount of material released was adapted for best image contrast. In most cases, 10 μm s⁻¹ scan speed, 10 Hz repetition rate, 100–150 μm spot size, resulting in a maximum fluence of 5 J cm⁻² were applied. The samples used were crystalline sodium chloride and pellets pressed from calcium dichloride powder, in the following referred to as calcium chloride.

Quantitative LA-ICP-MS analyses were done by LA of brass (MBH B26 from MBH Analytical Ltd., UK) and silicate glass (SRM NIST 610/612, National Institute of Standards and Technology (NIST), Boulder, CO, USA) by another ICP-QMS instrument (ELAN DRC Plus, Perkin Elmer, Waltham, MA, USA) tuned to optimum conditions for sensitivity and oxide formation rate, with the RF power set to 1350 W, the cooling and auxiliary gas flow rates to 17 and 0.75 L min⁻¹, respectively, and the extraction lens voltage to 7 V. For both the diagnostic measurements and quantitative analyses a ceramic injector of 2 mm inner diameter was chosen.

Aerosol wetting

In order to investigate to what extent the addition of water influences the vaporization of laser-produced aerosols in the ICP, ultrapure water was sprayed into a cyclonic spray chamber using a glass concentric nebulizer fed with approximately 0.7 mL min⁻¹ using a peristaltic pump operating at 11 rpm, as commonly done in solution nebulization (SN) ICP-MS. The wetted argon was then merged with helium behind the cell to keep the LA conditions unaffected. A sketch of the setup used for wetting laser-produced aerosols applying nebulization is shown in the left panel of Fig. 3.

For specifying the minimum amount of water which is required to observe changes in atomic emission profiles and, therefore, the vaporization process of laser-produced aerosols in the ICP, an alternative way of wetting the carrier gas in smaller doses became necessary. Thus, a micro-droplet dispenser (MD-K-150, Microdrop Technologies GmbH, Nordstedt, Germany) was used in combination with a vertically arranged droplet delivery assembly, as described in ref. 10 and 11 to supply precise quantities of water to the ICP, along with laser-produced aerosols (see the right panel of Fig. 3). Through

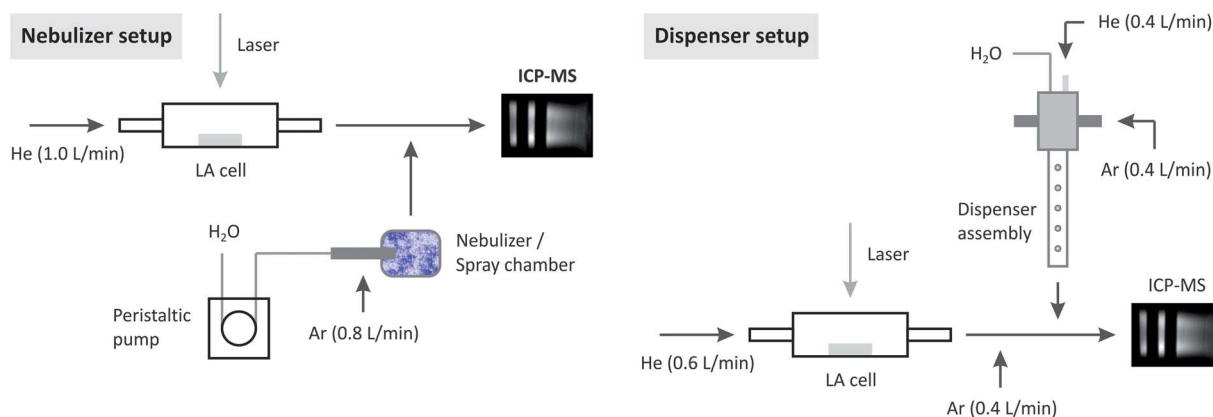


Fig. 3 Left panel: LA and carrier gas wetting using a nebulizer and spray chamber. Right panel: LA and carrier gas wetting using a micro-droplet dispenser.

1 varying the droplet ejection frequency from 100 to 1000 Hz and
 2 determining the size of droplets formed that ranged from about
 3 65 to 75 μm the exact amount of water added per unit of time
 4 could be calculated even for very small amounts. It should be
 5 emphasized that a similar precision would have not been
 6 achievable for the nebulizer/spray chamber system used since
 7 comparable amounts of water were impossible or difficult to
 8 weigh. For a better comparison of data, gas flows of 1.0 L min^{-1}
 9 helium and 0.8 L min^{-1} argon chosen in the previous experi-
 10 ments were kept. However, gases needed to be supplied through
 11 four mass flow controllers which resulted in an increased
 12 uncertainty of approximately 10% when adjusting the over-all
 13 flow rate.

15 Image and data processing

16 Image processing was carried out by Fiji¹³ and ImageJ;¹⁴ both
 17 are open source image processing tools for microscopy. For
 18 time-integrated OES measurements using the ICCD camera, at
 19 least three images were averaged to improve the signal-to-noise
 20 ratio. After that, a background image of the unloaded plasma
 21 but otherwise identical conditions was subtracted to obtain the
 22 element-specific emission. For images with a sufficient quality
 23 and contrast – as determined by eye inspection – background
 24 correction was performed by subtracting the emission observed
 25 close to the target wavelength which was obtained from the
 26 same image. Size calibration was done by image defocusing and
 27 monitoring of the RF coil, as mentioned above. All images of
 28 one experiment were acquired using identical zoom settings
 29 and, therefore, the same pixel size calibration was applicable to
 30 each set of images. To correct for variations in the image posi-
 31 tion on the entrance slit, the position of the RF coil was located
 32 and pictures were shifted accordingly. Emission profiles of the
 33 central channel were obtained from background-subtracted
 34 frames by integrating radially over a width of about the size of
 35 the outer diameter of the injector tube, *i.e.* 4 mm. For images
 36 acquired with water entrainment by nebulization, the positions
 37 of maximum axial emission were located using the “Find
 38 maxima” function provided by the Fiji software. The central
 39 channel around this point was then integrated over an axial
 40 width of 0.3 mm. In the case of low-volume water supply using
 41 the micro-droplet dispenser, axial maxima were identified by
 42 Gaussian fits of the emission profiles.

43 Results and discussion

44 Aerosol wetting using a nebulizer

45 Side-on imaging using the system described above allowed
 46 gaining further insights into the evaporation of aerosols
 47 produced by LA of solid materials. In particular, the possibility
 48 to switch between elements on-the-fly enabled us to monitor,
 49 *e.g.*, the residual water content by acquiring the hydrogen
 50 emission under wet and dry conditions. To investigate the effect
 51 of wetted carrier gases on atomic emission maps, sodium
 52 chloride and calcium chloride were ablated in helium and
 53 nebulized water was admixed in front of the ICP. Time-inte-
 54 grated and background-subtracted 2D emission images

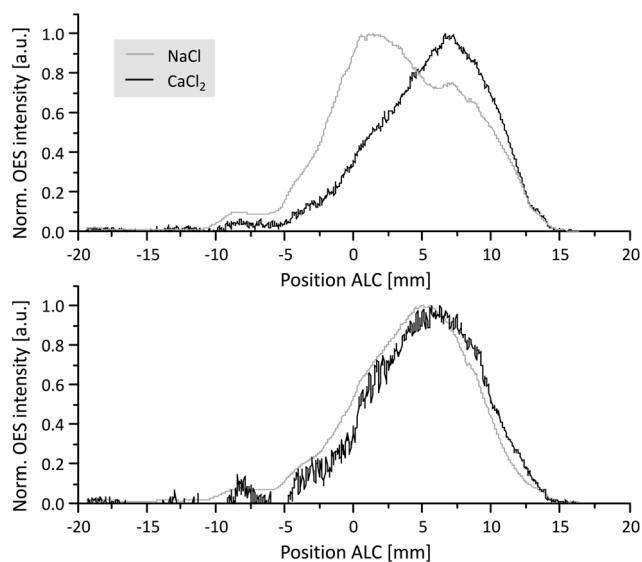


Fig. 4 Central axial emission profiles acquired for LA of sodium chloride and calcium chloride under dry plasma conditions (top panel) and during the addition of water using a concentric nebulizer (bottom panel). The profiles were integrated over a width of 4 mm and normalized with respect to maximum intensity values for better comparison. Positions are given as millimeter above load coil (ALC).

45 acquired this way were integrated radially over a width of 4 mm
 46 and centered on the injector–sampler axis. The resulting
 47 emission profiles were plotted on the same axis by defining the
 48 origin of the abscissa at the edge of the last RF coil turn to be the
 49 origin of the abscissa, as shown in Fig. 4. In the following,
 50 distances directing downstream this scale origin are referred to
 51 as “above load coil” (ALC). As can be seen, the addition of water
 52 resulted in a merging of the axial emission profiles.

53 Adding water, however, did not only have influence on the
 54 axial position of maximum atomic emission, which can be
 55 assumed to be the point of complete vaporization, as proposed
 56 in a recent paper.¹ In fact, adding water also lead to a widening
 57 of the radial distribution at the position of the axial emission
 58 maximum (see Fig. 5). This effect cannot be caused by a
 59 different starting point of vaporization because this would
 60 rather result in a narrowing as sodium chloride appears to
 61 vaporize earlier under dry plasma conditions (see Fig. 4).
 62 Assuming that diffusion is the main mechanism for the radial
 63 expansion of atoms and that for a given sort of atoms and
 64 constant pressure diffusion is mainly controlled by the gas
 65 temperature, a steeper temperature gradient would result in a
 66 faster expansion and would, thus, explain the data shown.
 67 Further, it can be assumed that a shortening of the steep
 68 temperature jump along the ICP axis was responsible for the
 69 matching of vaporization points because varying melting points
 70 of different species† would be reached over a much shorter
 71 distance.

† Since the chemical form of Na and Ca in the ICP is unknown chlorides as well as oxides have to be considered. However, Na has the lower boiling point (NaCl: 1700 K vs. CaCl₂: 2100 K; Na₂O: 1500 K vs. CaO: 3100 K) in both cases.

The formation of such a shortened temperature jump region in the presence of water can be a result of following mechanisms: adding water in large amounts provokes cooling along the central channel if the RF power is kept constant.¹⁵ This cooling may also lead to a shift in the onset of the steep temperature increase downstream, *i.e.* towards the sampler cone. Moreover, due to a better heat conductivity in the presence of gaseous water and a higher ion density,¹⁶ which enables a more efficient coupling to the RF field, a faster heating may be achieved. In our opinion, this shortened temperature jump region is the reason for the matching of positions of complete vaporization for substances with different boiling points. Further, the shortening of the temperature jump region would result in a faster radial expansion at this position.

Aerosol wetting using a micro-droplet dispenser

The determination of the amount of water necessary to obtain a significant shift and, ultimately, an overlap of the positions of maximum emission intensity required a precise admixture, which was not possible when using the nebulizer due to a missing real-time control of the precise amount of water exiting the attached spray chamber. Therefore, the water content was adjusted by a micro-droplet dispenser allowing for a supply of water with relative precisions better than 14% by altering the droplet ejection frequency in a range between 100 and 1000 Hz resulting in different degrees of wetness of the aerosol that entered the ICP, ranging from zero to 40% relative humidity at room temperature.[‡] The emission produced by evaporating particles was monitored and the axial emission maxima – as determined by Gaussian fits of the radially integrated emission profiles – were then plotted along with the signal intensities observed with the QMS *vs.* the water content added (see Fig. 6). It should be stressed that because of varying experimental conditions only the emission profiles in the case of sodium could be evaluated while data for calcium had to be discarded as most of the acquired frames had a signal–noise ratio too poor to perform reliable fits.[§] In Fig. 6, OES and QMS data are plotted and indicate that even very small amounts of water (<1 mg L⁻¹) had a strong impact on the emission profile shifts but not as much on the QMS signal intensity. The QMS signal became substantially reduced above water flow rates greater than 2 mg L⁻¹, corresponding to 10% relative humidity, at which the maximum had already shifted by 1 mm towards the sampler cone.

[‡] Higher levels of humidity could not be adjusted but may be achieved when operating dispenser units with larger nozzle diameters permitting to produce larger droplets and/or to raise their ejection frequency. However, a controlled increase of the water delivery rate by setting the ejection frequency to values larger than 1000 Hz failed because of dispenser instabilities resulting in the production of droplets of random number, size, and velocity which made an accurate determination of up-take rates impossible. Alternatively, inkjet printer cartridges may be used as a droplet dispenser unit¹⁷ which would also allow supplying increased water contents.

[§] By comparison, settings applied to 2D OES carried out for the nebulizer-based water supply were kept constant and the image contrast could be optimized accordingly.

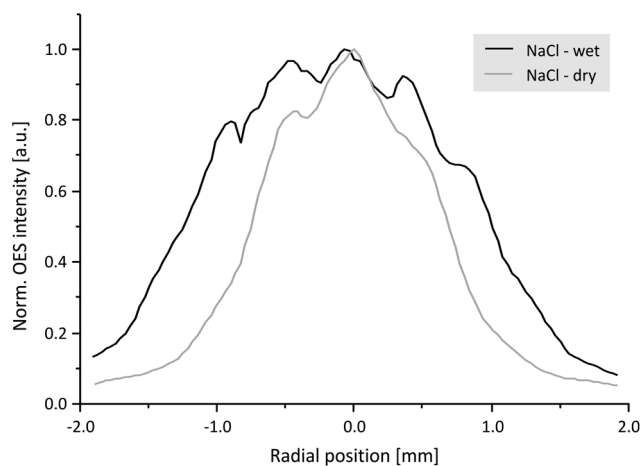


Fig. 5 Radial emission profiles for sodium chloride under dry and wet plasma conditions at the axial position of maximum emission. The profiles were integrated axially over a width of 0.3 mm and normalized with respect to maximum intensity values.

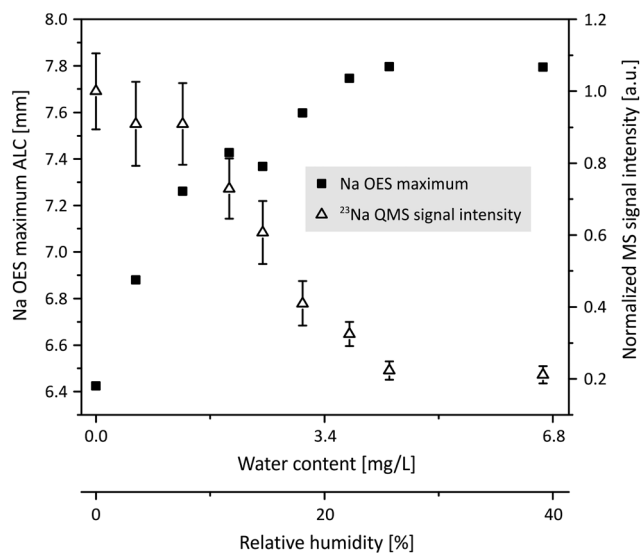


Fig. 6 Position of the axial emission maximum observed for sodium and QMS signal intensity plotted against the mean relative humidity and corresponding water content. Water contents were derived from droplet sizes and frequency of ejection. Note, that the positions of maximum emission achieved for contents larger than 3.4 mg L⁻¹ are slightly below values specified for water nebulization which, most probably, was due to the uncertainty of gas flow rate rates (see the Experimental section).

The different trends observed in the evolution of the emission maximum and QMS signal intensity with increasing water content were most likely due to processes relevant to the respective modes of detection: while changes in the OES profile are apparently a consequence of axial shifts of vaporization starting points and local variations of the excitation temperature *etc.*, QMS signal intensities are also determined by the ionization efficiency occurring further downstream the ICP. At first glance, the shift of the vaporization starting point towards the sampler cone should have allowed the increase of the QMS

signal intensity due to a retarded out-of-axis diffusion. However, the progressively reduced ionization efficiencies in front of the sampler cone at higher levels of humidity apparently over-compensated this effect, thus, giving decreased signal intensities under conditions which were not optimized for QMS up to that point (see the next section).

For water contents larger than about 3.4 mg L^{-1} , corresponding to 20% relative humidity, the axial position of maximum emission became nearly unchanged suggesting vaporization point matching to be accomplished and, therefore, any value above to be acceptable for improving the accuracy of LA-ICP-MS analyses. To avoid an excessive formation of interfering oxides and other polyatomic species while maintaining the higher degree of accuracy, humidity should be adjusted to values in this approximate range. For this reason, wetting of carrier gases by standard nebulizers is less advisable since it usually goes beyond water contents required unless the flow is split. Please note, that the specified range of humidity is approximate because it was determined for a specific ICP torch design, instrument-dependent power and flow rate settings *etc.*, and using the example of sodium. It may, thus, vary when other ICP-MS instrumentation is used or analytes of differing thermodynamic properties are monitored.

LA-ICP-QMS performance

The data presented in the previous section suggest a reduced amount of water to be sufficient for matching aerosol penetration depths and should, therefore, allow for similar improvements in the quantification capabilities as reported for LA-ICP-MS using standard nebulizer/spray chamber systems. To prove whether this suggestion was valid for quantitative LA-ICP-QMS analyses of SRM NIST 612 vs. SRM NIST 610 and MBH B26 vs. SRM NIST 610 applying matrix matched as well as unmatched calibration, respectively, were performed under dry and low humidity plasma conditions. For the latter, the amount of water supplied to the ICP was kept at an approximate level of 20%. In both cases, SRM NIST 610 served as external and ^{42}Ca as internal standard.

Analyzing brass on the basis of a non-matrix matched calibration by silicate glass standards represents a “worst case” scenario which according to the literature^{18–20} and our own experience can result in quantification errors exceeding 50% if LA is accomplished by ns lasers applying moderate fluences. Even though this inaccuracy is known to mainly be caused by non-stoichiometric LA,²¹ one can assume that differences in the penetration depths of metallic and dielectric aerosols and, thus, varying diffusion losses previously discussed also contribute. In consequence, a merging of penetration depths by the addition of water would permit equalizing relative diffusion losses and to estimate the range of this contribution.

Average precisions achieved for analyses of SRM NIST612 by matrix matched calibration under wet conditions turned out to be similar compared to those found using dry conditions whereas accuracies slightly worsened by about 5%; an outcome which we attributed to a residual number of incompletely vaporized particles when water was present and, to a minor

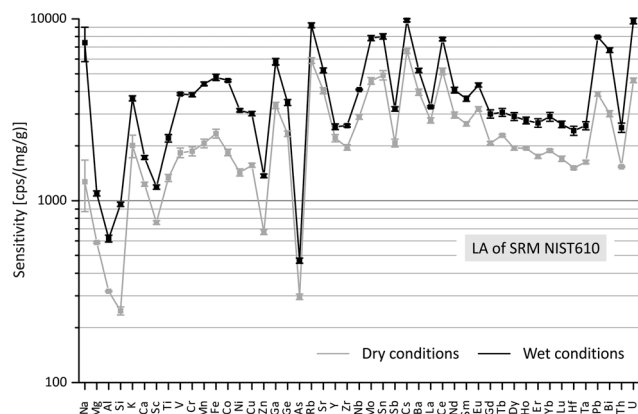


Fig. 7 Abundance-corrected sensitivities of elements measured by LA-ICP-QMS of SRM NIST 610 using wet and dry plasma conditions. The sensitivity pattern for the rare earth elements is unusual but is, most likely, due to an incomplete vaporization of micrometer sized particles which are known to be formed during LA at a wavelength of 266 nm, as performed here.

extent, the occurrence of spectral interferences through an increased oxide formation rate level specified to 1.7% ThO/Th. In fact, ns-LA performed at wavelengths equal or larger than 213 nm was recently demonstrated to occasionally result in the production of aggregates too large to be completely decomposed²² owing to coagulation and the short, approximately one millisecond lasting residence time in the hot zone of the ICP. In contrast, the merging of aerosol penetration depths in the case of MBH B26 brass analyses – quantified on ^{66}Zn using ^{65}Cu as internal standard – was not much affected by such detrimental effects and resulted in an accuracy improvement from initially 58% to a value of 49%, giving proof to the assumption made.

Another observation worth mentioning is the systematic improvement of sensitivities over the entire mass range for LA-ICP-QMS of both sample materials when water was supplied in small quantities, as can be seen in Fig. 7. This finding is consistent with data reported in ref. 4 which were collected at unknown levels of humidity, though.

Conclusion

We reported on the monochromator-based 2D OES imaging of analytes along the axis of an ICP formed by the vaporization of LA-produced aerosols under dry conditions and varying humidity. A spectral bandwidth of about 1.5 nm was achieved, which is a factor of 6 to 7 better than values offered by interference filters commonly applied for 2D OES imaging. The narrowing of the bandwidth enabled us to reduce the risk of spectral interferences and, in addition, resulted in a lowering of the background emission intensity. In the course of our study, 2D atomic emission patterns of sodium and calcium were acquired and 1D axial as well as radial emission profiles were computed from these patterns. A superposition of calcium- and sodium-specific axial OES profiles was observed in the presence of water. The maxima of these profiles were separated by several millimeters otherwise, *i.e.* when no water was added. These

findings provided a basis for the understanding and interpretation of results published by Günther *et al.*⁴ and O'Connor *et al.*⁵ who showed sensitivity and accuracy improvements of LA-ICP-MS analyses upon water addition. According to a hypothesis recently made these improvements may be due to a matching of so-called aerosol penetration depths or, more precisely, the analyte/material-dependent positions of complete vaporization and, therefore, an adaptation of material losses in consequence of out-of-axis diffusion.¹ Assuming the positions of maximum atomic emission to be the starting points of diffusion, the superposition of axial OES profiles observed can be considered a proof for this hypothesis. We attribute the matching of analyte-dependent points of vaporization to an increased temperature gradient formed along the ICP axis or, in other words, a confinement of the region in which the gas temperature jumps from room temperature to its maximum.²³

Two different water introduction systems – a nebulizer and a micro-droplet dispenser – were used and the latter allowed specifying the approximate amount of water and the corresponding level of humidity required for matching vaporization points. With the conditions set and instrumentation chosen, a minimum level of relative humidity of around 20–30% was determined. We concluded to not go too far beyond this range in order to keep oxide formation low, which suggests the utilization of common nebulizer/spray chamber systems to be less adequate since those were found to oversupply the amount of water needed. In comparison, the usage of a micro-droplet dispenser equipped with an observation assembly enables one to precisely dose the amount of water entrained into the ICP.

To clarify if a reduced level of humidity would still be sufficient to maintain the improved quantification capabilities LA-ICP-MS offers upon water addition, analyses of brass by non-matrix matched calibration using silicate glass standards were carried out. In doing so, a systematic enhancement of sensitivities as well as accuracy improvements of nearly 10% was found. These findings are consistent with data reported by Wälle *et al.*⁷ who showed that accuracies improve by up to 30% when switching from dry to wet conditions. The values reported here can, therefore, be considered an estimation of the relative portion of fractionation originating from the ICP if matrix matching cannot be applied.

Acknowledgements

Financial support by the Swiss National Science Foundation (SNSF, project ID 141292) is gratefully acknowledged. We thank Daniel Frick for his help in setting up the optical system, Roland Mäder from the mechanical workshop of the Laboratory of Inorganic Chemistry (LAC) of ETH for manufacturing important pieces of our equipment, and Olga Borovinskaya for operating the micro-droplet dispenser. In addition, we would like to thank Prof. K. Niemax and Dr R. Hergenröder for providing the monochromator used in this work.

References

- 1 L. Flamigni, J. Koch and D. Günther, *Spectrochim. Acta, Part B*, 2012, **76**, 70–76.
- 2 R. E. Russo, X. Mao, J. Gonzalez, V. Zorba and J. Yoo, *Anal. Chem.*, 2013, **56**, 1375–1386.
- 3 S. F. Durrant, *J. Anal. At. Spectrom.*, 1999, **14**, 1385–1403.
- 4 D. Günther and C. A. Heinrich, *J. Anal. At. Spectrom.*, 1999, **14**, 1363–1368.
- 5 C. O'Connor, B. L. Sharp and P. Evans, *J. Anal. At. Spectrom.*, 2006, **21**, 556–565.
- 6 B. Fryer, S. Jackson and H. Longerich, *Can. Mineral.*, 1995, **33**, 303–312.
- 7 M. Wälle, J. Koch and D. Günther, *J. Anal. At. Spectrom.*, 2008, **23**, 1285–1289.
- 8 A. Murtazin, S. Groh and K. Niemax, *Spectrochim. Acta, Part B*, 2012, **76**, 3–16.
- 9 J. W. Olesik and G. M. Hieftje, *Anal. Chem.*, 1985, **57**, 2049–2055.
- 10 M. R. Webb and G. M. Hieftje, *Appl. Spectrosc.*, 2006, **60**, 57–60.
- 11 S. Gschwind, L. Flamigni, J. Koch, O. Borovinskaya, S. Groh, K. Niemax and D. Günther, *J. Anal. At. Spectrom.*, 2011, **26**, 1166–1174.
- 12 J. Koch, L. Flamigni, S. Gschwind, S. Allner, H. Longerich and D. Günther, *J. Anal. At. Spectrom.*, 2013, DOI: 10.1039/c3ja50052g.
- 13 J. Schindelin, I. Arganda-Carreras, E. Frise, V. Kaynig, M. Longair, T. Pietzsch, S. Preibisch, C. Rueden, S. Saalfeld, B. Schmid, J.-Y. Tinevez, D. J. White, V. Hartenstein, K. Eliceiri, P. Tomancak and A. Cardona, *Nat. Methods*, 2012, **9**, 676–682.
- 14 C. A. Schneider, W. S. Rasband and K. W. Eliceiri, *Nat. Methods*, 2012, **9**, 671–675.
- 15 J. Schafer, W. Lyons, W. G. Tong and P. M. Danehy, *Appl. Phys. B*, 2009, **95**, 161–168.
- 16 A. Montaser, *Inductively coupled plasma mass spectrometry*, Wiley-VCH, 1998.
- 17 J. O. O. v. Niessen, J. N. Schaper, J. H. Petersen and N. H. Bings, *J. Anal. At. Spectrom.*, 2011, **26**, 1781–1789.
- 18 C. Liu, X. L. Mao, S. S. Mao, X. Zeng, R. Greif and R. E. Russo, *Anal. Chem.*, 2003, **76**, 379–383.
- 19 J. Koch, A. von Bohlen, R. Hergenröder and K. Niemax, *J. Anal. At. Spectrom.*, 2004, **19**, 267–272.
- 20 E. F. Cromwell and P. Arrowsmith, *Appl. Spectrosc.*, 1995, **49**, 1652–1660.
- 21 R. Glaus, R. Kaegi, F. Krumeich and D. Günther, *Spectrochim. Acta, Part B*, 2011, **65**, 812–822.
- 22 D. Fliegel, M. Klementova and J. Kosler, *Anal. Chem.*, 2010, **82**, 4272–4277.
- 23 G. C. Y. Chan, W. T. Chan, X. Mao and R. E. Russo, *Spectrochim. Acta, Part B*, 2001, **56**, 1375–1386.